Bending stability of $Cu_{0.4}CrO_2$—A transparent p-type conducting oxide for large area flexible electronics

E. Norton ⓘD, L. Farrell ⓘD, A. Zhussupbekova, D. Mullarkey ⓘD, D. Caffrey ⓘD, D. T. Papanastasiou ⓘD, D. Oser, D. Bellet, I. V. Shvets, and K. Fleischer ⓘD

View Online   Export Citation   CrossMark

ARTICLES YOU MAY BE INTERESTED IN

Bending stability of $Cu_{0.4}CrO_2$—A transparent p-type conducting oxide for large area flexible electronics

E. Norton,[1] L. Farrell,[1] A. Zhussupbekova,[1] D. Mullarkey,[1] D. Caffrey,[1,2]
D. T. Papanastasiou,[3] D. Oser,[3] D. Bellet,[3] I. V. Shvets,[1,2] and K. Fleischer[1,2,a]

[1]*School of Physics and Centre for Research on Adaptive Nanostructures and Nanodevices (CRANN), Trinity College, University of Dublin, Dublin 2, Ireland*
[2]*Advanced Materials and BioEngineering Research (AMBER), Trinity College, University of Dublin, Dublin 2, Ireland*
[3]*Univ. Grenoble Alpes, CNRS, Grenoble INP, LMGP, F-38000 Grenoble, France*

The current best performing p-type transparent conducting oxides are typically highly crystalline materials, deposited at high temperatures, and hence incompatible with the drive to low cost flexible electronics. We investigated a nanocrystalline, copper deficient Cu_xCrO_2, deposited at low temperatures upon a flexible polyimide substrate. The as-deposited film without post annealing has an electrical conductivity of $6 Scm^{-1}$. We demonstrate that this p-type transparent oxide retains its excellent electrical conductivity under tensile strain, withstanding more than one thousand bending cycles without visible cracks or degradation in electrical properties. In contrast, compressive strain is shown to lead to an immediate reduction in conductivity which we attribute to a de-lamination of the thin film from the substrate. © *2018 Author(s). All article content, except where otherwise noted, is licensed under a Creative Commons Attribution (CC BY) license (http://creativecommons.org/licenses/by/4.0/).* https://doi.org/10.1063/1.5027038

In many optoelectronic devices the electrodes and contact materials are metallic. Some applications (displays and thin film solar cells among others) require materials that are transparent yet electrically conductive. To date, such transparent electrodes are made from doped metal oxides, most commonly *n*-type Indium Tin Oxide (ITO).[1,2] Today, there is great scope for flexible electronic devices, e.g., printed solar cells, to complement the mature silicon based electronic industry.[3] The electrical conductivity of ITO is strongly linked to its long range crystalline order. ITO is quite brittle and often cracks on polymeric substrates under a low strain when deposited over large areas, thus it has shown sub par performance on flexible substrates.[4,5]

n-type amorphous transparent semiconducting oxides such as Indium Gallium Zinc Oxide (IGZO) satisfy the basic criteria required for flexible devices: highly conductive when deposited at low temperatures.[6] Its amorphous nature avoids the complexities and variability of its polycrystalline counterpart, ITO.

Analogous *p*-type Transparent Conducting Oxides (TCOs) have only found uses in laboratory devices, e.g., buffer layers in dye sensitized solar cells, hole injectors in organics light emitting diodes, water splitting electrodes, and as new generation of transparent electrical contacts for p-type semiconductors.[7–10]

With an outlook towards cheap printable electronics these test devices will become industrially relevant if a well performing p-type TCO for hole injecting layers, transparent p-n junctions and consequently transparent electronics is found. In addition to identifying a material itself, roll to roll processing of devices requires materials that can withstand tensile strain even if the active device will not be flexible. However, most *p*–type TCOs are polycrystalline with processing temperatures in excess of 600°C, which is too high for use with flexible substrates. Only one amorphous *p*-type

---

[a]Electronic mail: fleisck@tcd.ie

TCO has been synthesised so far: Zinc Rhodium Oxide.[11,12] Its relatively low conductivity at room temperature ($0.14 Scm^{-1}$) is however not sufficient for applications as a transparent electrode.

An alternative material, *p*-type Cu_xCrO_2 has recently been synthesised by solution processed methods as well as chemical vapour deposition (CVD) in a temperature regime that is compatible with flexible plastics.[13–18] Interestingly, Cu_xCrO_2 retains its high electrical conductivity without the need for crystalline order above the nanoscale range.

Here we investigate the performance of optimised p-type $Cu_{0.4}CrO_2$ as a part of a flexible p-type transparent electrode. $Cu_{0.4}CrO_2$ films were grown via spray pyrolysis on Kapton® DuPont HN Polyimide film (thickness 80 μm). Following previously optimised growth conditions for thicker films (90nm),[14] copper acetylacetonate and chromium acetylacetonate precursors were dissolved in methanol and sprayed with an air blast nozzle (PNR, model MAD-0331) using a mixture of compressed air/nitrogen (5%/95%) with a gas flow rate of 17L min^{-1} onto heated (345°C) polyimide film. The molarity (*M*), spray time (*t*), and solution flow (*f*) was adjusted to control the film thickness and optimise conductivity; 90±10 nm: M_{Cr}=30 mM, M_{Cu}=12 mM, *t*=20 min, *f*=1.7 ml/min; 25±10 nm: M_{Cr}=10mM, M_{Cu}=4 mM, *t*=17 min, *f*=1.7 ml/min. The Kapton substrate rested on microscope slides which lay on the hot plate surface to achieve a comparable substrate temperature to previously optimised growth runs directly on glass. Heater surface temperature readings during growth were taken using a type K thermocouple (chromel vs. alumel) welded to the top of the hot plate. The temperature was PID controlled during growth to 345 ± 10°C. The surface temperature at the substrate may have systematically differed. As-grown films on glass (90nm) show a copper content of ~35% as determined by X-ray photoelectron spectroscopy, a sheet resistance of $20k\Omega^{-2}$, conductivity of $20Scm^{-1}$ and a carrier activation energy of 200meV. The sheet resistance was determined by 4 point probe (4PP) measurements, the carrier activation energy from Arrhenius fits on 4PP measurements from 50 to 150°C. Films grown on Kapton have similar carrier activation energies (200-250meV), with sheet resistance of 60 ± 10 $k\Omega^{-2}$, 350± 100 $k\Omega^{-2}$ for the sample sets of 90 and 25nm. In our system it is more difficult to maintain optimised growth conditions over a larger area for Kapton compared to glass, due to the difficulties in homogeneously heating the thin plastic substrates under the high pressure gas flow. Consequently films on Kapton have lower conductivities than those on glass.

All resistance measurements in the bending study are done by simple 2 point contact measurements. The carrier mobility of the films is too low for Hall measurements and is expected to be as low as similar films prepared on glass substrates where estimations by Seebeck measurements gave hole mobilities of $0.006cm^2$/Vs and high carrier concentrations of ($2.5 \times 10^{22}cm^{-3}$).[14,19]

The current work is limited to sets of 25 nm and 90nm thick films grown at 345°C on polyimide, as the growth window for well performing spray pyrolysis grown Cu_xCrO_2 is very narrow. At temperatures below 320°C the precursors do not decompose and no growth is observed, while at higher temperatures a) the conductivity decreases due to the formation of Cr_2O_3:Cu and b) no stable flexible substrate for the bending tests are available. Hence, detailed temperature dependent studies are not feasible. Likewise the thickness dependence of the bending stability was only studied in a narrow range. For the intended application as flexible hole transport layer in, e.g., organic solar cells an oxide thickness of typically 10nm is used.[20] However the inherent roughness of spray pyrolysis grown films, combined with the need for a sheet resistance below $500k\Omega^{-2}$ in the bending setup, limits the thickness range we could investigate. We will demonstrate no film degradation for our maximum applicable tensile stress in one order of magnitude thicker layers (80 - 100nm), with some degradation for thinner layers. We wish to stress that the results could be improved by the use of alternative growth techniques shown to lead to better homogeneity, lower roughness and higher conductivity.[16–18] Indeed in MOCVD grown $Cu_{0.4}CrO_2$ a conductivity of up to $100Scm^{-1}$ has been reported, an order of magnitude higher than achievable with our low cost spray pyrolysis. Even with this limitation conductivities are significantly higher than for other p-type TCOs compatible with plastic substrates such as SnO_x and a-$ZnRhO_4$.[15,21–23]

Figure 1a shows Grazing Incidence X-ray diffraction (GIXRD) of a typical sample (90nm). XRD measurements were performed on a Bruker D8 Advance diffractometer using a Cu K_α source with a double bounce Ge monochromator. The GIXRD scan was collected with a grazing incidence angle of 1° using a large copper soller slit and a scintillation detector. The (006) reflex for $CuCrO_2$ is notably
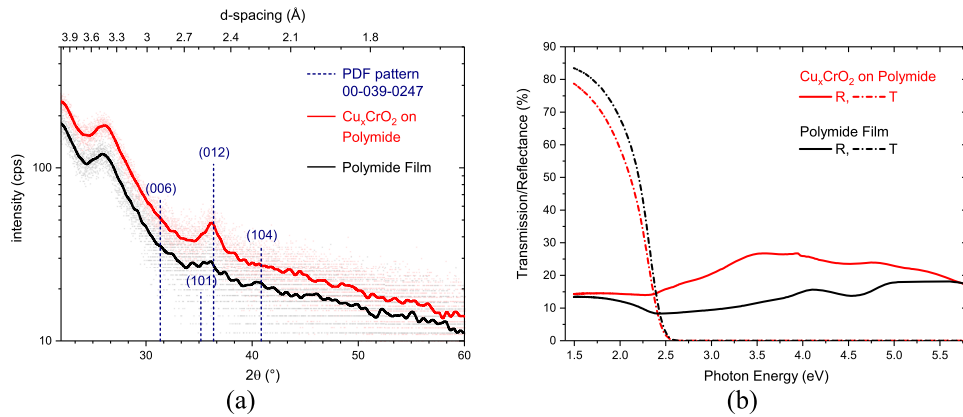
FIG. 1. (a) Grazing incidence x-ray diffraction of a typical $Cu_{0.4}CrO_2$ sample grown on polyimide compared to bare polyimide film. Only a broad, weak (012) reflex of $CuCrO_2$ (PDF-00-39-247) is observed, indicating the poor crystallinity (< 7nm grain size) and preferential crystallographic orientation of these films. (b) Ultra Violet-Visible Spectroscopy (Transmission T and Reflectance R) of $Cu_{0.4}CrO_2$ grown upon polyimide film and the bare polyimide substrate as reference. The sample was illuminated from the thin film side for T and R.

absent: indicating either a randomly ordered CrO_6 environment or a strong crystallographic texture of the film. The weak (012) reflex is likewise attributed to ordering of the O-Cu-O planes on the nanometre scale due to the peculiarities of the spray pyrolysis growth.[14] Many chromium-containing p-type oxides possess a CrO_6 edge network similar to that of Rh_2O_3 in Zinc Rhodium Oxide. This edge sharing network of RhO_6 octahedra in zinc rhodium oxide is quite insensitive to distortion in an amorphous state.[11] We have previously shown that the valence band of chromium based TCOs is dominated by states localised in the CrO_6 octahedra with a low mobility conduction involving an electron hopping mechanism.[19,24] Hence, the nanocrystalline nature of the films combined with a valence band state related to a disordered CrO_6 edge sharing network leads to the observed resilience of the films to tensile strain discussed below.

Figure 1b shows the optical transmittance and reflectance of a $Cu_{0.4}CrO_2$ film grown upon polyimide film. The bare polyimide film itself absorbs strongly above a photon energy of 2.5eV. This is below the onset of strong absorption in Cu_xCrO_2 and thus no additional absorption is introduced by the film. The indirect gap of $Cu_{0.4}CrO_2$ was determined previously to be 2.4±0.1eV.[15] The $Cu_{0.4}CrO_2$, grown with thickness 90nm, does not detrimentally affect the transmittance when grown upon the bare polyimide film beyond a minor reflectance increase due to the addition of a film with higher refractive index onto the substrate.[15]

To test the suitability of these films as a large area flexible electrode the change in the electrical resistance after mechanical tensile and compressive strain was investigated. As the underlying substrate is insulating, the change in electrical resistance is solely a measure of the structural changes in the conductive oxide layer induced by the applied mechanical stress. This is equivalent to previously bending tests in n-type TCOs.[25]

I. TENSILE STRAIN

One folding cycle consists of bending the sample so that the distance between the two electrical contacts decreases from the unfolded value, 31.5 mm. The minimum distance possible between the two contacts was 3.3 mm. If the sample is bent upwards in a ∩-shape tensile stress is applied to the thin conducting film. Figure 2 shows the procedure schematically, as well as photos of the experimental setup at each stage of the bending cycle. The automated electrical resistance measurements were taken whenever the sample was in the unfolded position. Initial, manual bending measurements taken with two point electrical measurements at 5 mm bending radius showed no difference between bent and unbent resistance (see Fig. 2).

A side profile image was taken of the folded film at the maximum bending point. The software ImageJ[26] was then used to estimate the minimum radius of curvature, illustrated in Figure 2a. The
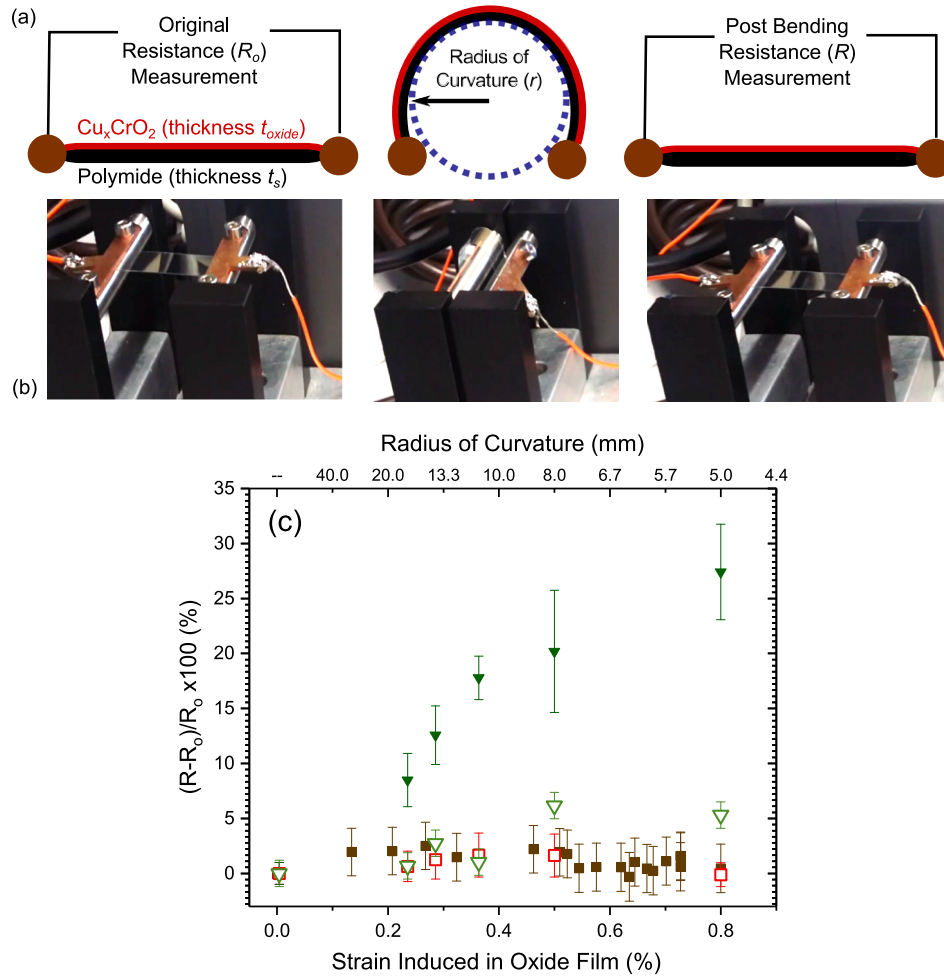
FIG. 2. (a) Schematic of one tensile strain bending cycle. The analogous compressive stress is applied when the film is bent in a ∪-shape (b) Images of the apparatus at each stage of the bending cycle. (c) normalised change in electrical resistance ($R - R_o)/R_o$ as function of applied stress in an 90nm thick $Cu_{0.4}CrO_2$ oxide film. Automated electrical measurements for tensile strain were made after the induced strain had been released from the film (■). Additional manual measurements of $(R - R_o)/R_o$ during application of tensile (□) as well as during (▽) and after (▼) compressive strain.

oxide layers grown (25 - 90nm) are considerably thinner than the substrate. The neutral axis is very close to the centre of the composite. Therefore, strain distributed to the conductive oxide is given by:

$$\text{strain} = \epsilon = \frac{t_s + t_{\text{oxide}}}{2r} \approx \frac{t_s}{2r} \tag{1}$$

where t_s and t_{oxide} are the thickness of the substrate and conductive oxide films, respectively, and r is the radius of curvature. As the induced mechanical strain is dependent on the substrate thickness, plotting the change in electrical resistance as a function of the radius of curvature after each bending cycle is therefore not an absolute comparison. Figure 2c shows the change in resistance of a $Cu_{0.4}CrO_2$ film as function of bending radius, and using equation (1) as function of induced strain. As no degradation was observed, even at the maximum accessible strain, all subsequent tests have been performed at maximum strain of 0.8% (minimum radius 5mm). To further increase strain, and possibly reach the stability threshold, Cu_xCrO_2 would need to be deposited on much thicker substrates.

Figure 3a shows the absolute resistance and normalised change in resistance for 2000 automated bending cycles inducing maximum tensile strain of 0.8%. For the thicker samples the resistance of $Cu_{0.4}CrO_2$ increased by 9% within the first 500 cycles and no further changes are observed for subsequent cycles. Thinner samples are more susceptible to degradation under tension and a more gradual increase in resistance of up to 25% was observed. Even though little change in electrical
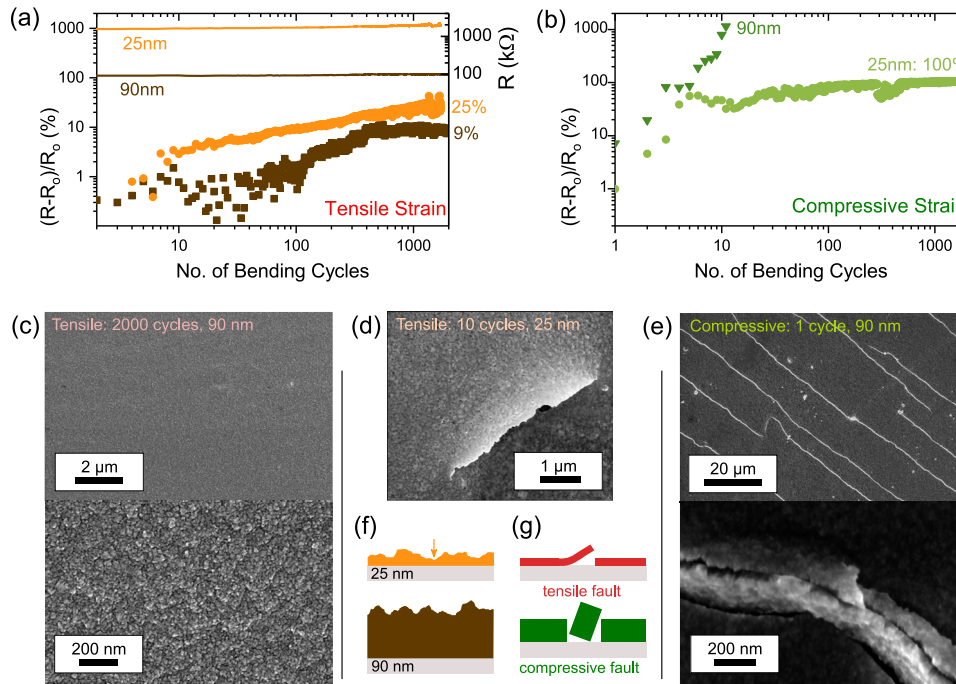
FIG. 3. (a) Resistance and normalised change in resistance ($(R - R_o)/R_o$) for successive tensile strain bending cycles of a 25nm (●) and 90nm (■) thick $Cu_{0.4}CrO_2$ film. The maximum applicable strain of 0.8% (r=5mm) was used. (b) $(R - R_o)/R_o$ of 25nm (●) and 90nm (▼) samples under equivalent compressive stress. The values for the compressive bending cycles saturate for the thicker sample at the operational limit of our electrical measurement system. (c) Scanning Electron Microscopy (SEM) of a 90nm sample on polyimide film after 2000 bending cycles. To expose potential cracking of the film the sample was mounted under equivalent tension; (d) Isolated delaminated area seen in a 25nm sample after 10 manual bending cycles (tension, 5mm). (e) Large scale (top) in SEM image of $Cu_{0.4}CrO_2$ on polyimide film after a single compressive strain cycle; the magnified SEM image (bottom) of a crack seen above. (f) Schematic of the sample morphology. The thinner samples are more susceptible to delamination, as the film roughness is comparable to the thickness, thus creating isolated weak points (see arrow). (g) Schematic of different morphology of faults created under compression and tension.

resistance was observed, the high initial resistance (91.6kΩ) of a $Cu_{0.4}CrO_2$ film may mask any structural degradation in the film. A thin film deposited on a flexible substrate under tension will reach a threshold where channeling cracks appear which allow partial relaxation of stress, eventually followed by buckling delamination.[27]

Scanning Electron Microscopy (SEM) images of the Cu_xCrO_2 film grown on polyimide are shown in Fig. 3c. The thicker film, imaged after having undergone over 2000 bending cycles was mounted mechanically bent with a 5mm radius consistent with that used in the bending tests. By mounting the films under tensile stress we can expose any thin channeling cracks. We were unable to observe any channeling cracks in our strained films. This indicates that we have not induced the threshold strain where cracking of the film occurs. In contrast the thinner film already shows isolated cases of delamination after a few bending cycles Fig. 3d, consistent with the more prominent change in resistance. As schematically illustrated in Fig. 3f in spray pyrolysis grown, nanocrystalline films the roughness is broadly independent of thickness, leading to an increased weakness against shearing of very thin films in random areas.

II. COMPRESSIVE STRAIN

In contrast to the stability of the thicker films under tensile strain, extensive compressive studies could not be performed due to limitations in the bending set-up. However, films that underwent manual compressive strain cycles (bending the sample down in a ∪-shape) showed large changes in electrical resistance, as shown in Fig. 3b. Subsequent SEM images show channelling cracks of the films treated this way (see Fig. 3e). A small scale image of a single crack shows that the film has

buckled upwards, indicative of a local delamination of the TCO layer. As these faults extend over the full width of the sample dramatic resistance changes are observed. In additional manual bending tests shown in Fig. 2, where resistance measurements during the bending cycle are possible, we also notice a stark difference between the bent and unbent case for compressive strain. The change in resistance is significantly smaller in the bent state compared to after the film was flattened again. This suggests that the side walls of the cracks (see Fig. 3e,g) remain in electrical contact in the bent state and only after flattening is the change in resistance observed, as flakes of the film delaminated in the bent state can fall out. This suggests that once the $Cu_{0.4}CrO_2$ films are embedded in a full device structure where there will be more layers above the film, stability under compressive stress could be better. While the cracking will still occur, the mechanical delamination and material fall-out could be reduced. The manual bending experiment also suggests a threshold for crack formation of ~0.1% or 20cm radius for the 90nm thick films used. Data points and error bars of the manual bending experiment are based on the average and variance between results of different samples. In contrast to the tensile measurements thinner films are slightly more stable under compressive stress and after the initial increase of 100%, further repeated bending do not further degrade the sample.

To summarise, sets of 25±10nm and 90±10nm thick $Cu_{0.4}CrO_2$ have been deposited upon flexible substrates. The deposited $Cu_{0.4}CrO_2$ is of comparable sheet resistance to films on glass, as well as other crystalline p-type oxides, even though they lack in long range crystalline order above the nanoscale, which many oxides need for good electrical conductivity. In our films, O-Cu-O planes are ordered within $\approx$ 7nm grains and the CrO_6 edge shared network is disordered. The $Cu_{0.4}CrO_2$ grown on polyimide film by spray has an electrical conductivity of $6Scm^{-1}$ which does not significantly degrade when put under tension. As little change was observed we can only give a lower limit for the strain threshold for the thicker films. There is a minor degradation upon repeated bending cycles in the thinner films at the maximum achieved strain of 0.8%. For compressive strain degradation was observed with a threshold of delamination at strain values of 0.1%. This work experimentally confirms that the nanocrystalline Cu_xCrO_2 is a suitable p-type TCO compatible with flexible electronics in general. The roughness of low cost spray pyrolysis grown films though, may limit the device performance and stability due to the unavoidable roughness of the films. Further growth equipment optimisations such as the use of sophisticated ultrasonic nozzles to minimise gas pressure, as well as more suitable heaters to achieve temperature homogeneity on thin plastic substrates may be required.

[1] J. F. Wager, Science **300**, 1245 (2003).
[2] K. Ellmer, Nature Photonics **6**, 809 (2012).
[3] Y.-B. Cheng, A. Pascoe, F. Huang, and Y. Peng, Nature **539**, 488 (2016).
[4] K. Alzoubi, M. M. Hamasha, S. Lu, and B. Sammakia, J. Disp. Technol. **7**, 593 (2011).
[5] D. R. Cairns, R. P. Witte, D. K. Sparacin, S. M. Sachsman, D. C. Paine, G. P. Crawford, and R. R. Newton, Appl. Phys. Lett. **76**, 1425 (2000).
[6] K. Nomura, H. Ohta, A. Takagi, T. Kamiya, M. Hirano, and H. Hosono, Nature **432**, 488 (2004).
[7] J. C. Bernede, S. Houari, D. Nguyen, P. Y. Jouan, A. Khelil, A. Mokrani, L. Cattin, and P. Predeep, Physica Status Solidi (a) **209**, 1291 (2012).
[8] C.-S. Chou, C.-M. Hsiung, C.-P. Wang, R.-Y. Yang, and M.-G. Guo, Int. J. Photoenergy **2010**, 1.
[9] I. D. Parker, J. Appl. Phys. **75**, 1656 (1994).
[10] D. S. Ginley and C. Bright, MRS Bull. **25**, 15 (2000).
[11] T. Kamiya, S. Narushima, H. Mizoguchi, K. Shimizu, K. Ueda, H. Ohta, M. Hirano, and H. Hosono, Adv. Funct. Mater. **15**, 968 (2005).
[12] S. Narushima, H. Mizoguchi, K. Shimizu, K. Ueda, H. Ohta, M. Hirano, T. Kamiya, and H. Hosono, Adv. Mater. **15**, 1409 (2003).
[13] L. Farrell, E. Norton, B. J. O'Dowd, D. Caffrey, I. V. Shvets, and K. Fleischer, Appl. Phys. Lett. **107**, 031901 (2015).
[14] L. Farrell, E. Norton, C. M. Smith, D. Caffrey, I. V. Shvets, and K. Fleischer, J. Mater. Chem. C **4**, 126 (2016).
[15] K. Fleischer, E. Norton, D. Mullarkey, D. Caffrey, and I. V. Shvets, Materials **10**, 1019 (2017).
[16] P. L. Popa, J. Crêpellière, R. Leturcq, and D. Lenoble, Thin Solid Films **612**, 194 (2016).

[17] J. Crêpellière, P. L. Popa, N. Bahlawane, R. Leturcq, F. Werner, S. Siebentritt, and D. Lenoble, J. Mater. Chem. C **4**, 4278 (2016).

[18] P. L. Popa, J. Crêpellière, P. Nukala, R. Leturcq, and D. Lenoble, Applied Materials Today **9**, 184 (2017).

[19] L. Farrell, K. Fleischer, D. Caffrey, D. Mullarkey, E. Norton, and I. V. Shvets, Phys. Rev. B **91**, 125202 (2015).

[20] J. Kettle, H. Waters, M. Horie, and S. Chang, Journal of Physics D: Applied Physics **45**, 125102 (2012).

[21] W. Guo, L. Fu, Y. Zhang, K. Zhang, L. Liang, Z. Liu, H. Cao, and X. Pan, Applied Physics Letters **96**, 042113 (2010).

[22] M. Dekkers, G. Rijnders, and D. H. Blank, Appl. Phys. Lett. **90**, 021903 (2007).

[23] A. R. Nagaraja, N. H. Perry, T. O. Mason, Y. Tang, M. Grayson, T. R. Paudel, S. Lany, and A. Zunger, J. Am. Ceram. Soc. **95**, 269 (2012).

[24] E. Norton, L. Farrell, S. Callaghan, C. McGuinness, I. Shvets, and K. Fleischer, Physical Review B **93**, 115302 (2016).

[25] A. Muthukumar, G. Giusti, M. Jouvert, V. Consonni, and D. Bellet, Thin Solid Films **545**, 302 (2013).

[26] C. A. Schneider, W. S. Rasband, and K. W. Eliceiri, Nature Methods **9**, 671 (2012).

[27] B. Cotterell and Z. Chen, Int. J. Fract. **104**, 169 (2000).